International Journal of Heat and Mass Transfer 52 (2009) 2390–2398

Contents lists available at ScienceDirect

International Journal of Heat and Mass Transfer

journal homepage: www.elsevier.com/locate/ijhmt

Heat, air and moisture transfer through hollow porous blocks

Gerson Henrique dos Santos *, Nathan Mendes

Thermal Systems Laboratory, Department of Mechanical Engineering, Pontifical Catholic University of Paraná – PUCPR, R. Imaculada Conceição, 1155, Curitiba-PR, 80.2+15-901, Brazil

ARTICLE INFO

Article history:
Received 10 June 2008
Received in revised form 5 November 2008
Available online 26 December 2008

Keywords:
Coupled heat and moisture transfer
Hollow elements
Porous material
Building simulation

ABSTRACT

The combined heat, air and moisture transfer in building hollow elements is of paramount importance in the construction area for accurate energy consumption prediction, thermal comfort evaluation, moisture growth risk assessment and material deterioration analysis. In this way, a mathematical model considering the combined two-dimensional heat, air and moisture transport through unsaturated building hollow bricks is presented. In the brick porous domain, the differential governing equations are based on driving potentials of temperature, moist air pressure and water vapor pressure gradients, while, in the air domain, a lumped approach is considered for modeling the heat and mass transfer through the brick cavity. The discretized algebraic equations are solved using the MTDMA (MultiTriDiagonal-Matrix Algorithm) for the three driving potentials. Comparisons in terms of heat and vapor fluxes at the internal boundary are presented for hollow, massive and insulating brick blocks. Despite most of building energy simulation codes disregard the moisture effect and the transport multidimensional nature, results show those hypotheses may cause great discrepancy on the prediction of hygrothermal building performance.

1. Introduction

Heat, air and moisture (HAM) transfer through porous media is explored in many engineering areas such as oil extraction, transport in textile materials [1], wood drying [2], pollutants infiltration, granular materials drying [3], heat exchangers [4], transport in composite membrane [5] and thermal insulation [6] among others. Therefore, in the construction area, detailed heat, air and moisture models are needed to increase the accuracy of heat and moisture transfer calculation between outdoor and indoor environments for better predicting thermal loads, indoor thermal comfort and air quality indices and mold growth risk.

For the thermal performance evaluation of building envelopes, the presence of moisture implies an additional latent heat transport that may cause great discrepancies on the indoor air temperature and humidity values [7]. Despite the importance, building envelope mathematical models are limited, mainly when air- and vapor-permeable hollow blocks are considered within the building walls.

Heat transfer through hollow blocks takes places simultaneously due to combined processes (radiation–convection–conduction) within its core. Although the coupled problem has received great attention currently, the available literature on the heat and moisture transfer of hollow porous elements is still limited. In hygrothermal whole-building performance analysis, a complete model including all phenomena becomes very complex and simulations very time consuming.

Concerning moisture transport, the first developed models were focused on the analysis of porous soils. Lewis [8], Richards [9], Phillip and DeVries [10] and Luikov [11] elaborated the first phenomenological models to characterize the transport in unsaturated porous media. In the building area, the first technique developed in the eighties to evaluate moisture in building materials was the well-known Glaser's method. Pedersen [12] and Kunzel [13] have developed more complete models that take into account the liquid and vapor diffusive transport. Mendes et al. [14] have developed a model based on the Philip and DeVries model to predict heat and moisture transfer through porous building elements.

In the citations mentioned above, only massive elements have been considered. Nevertheless, cavities in building hollow elements may play a very important role on the hygrothermal performance so that convective transport coefficient values for different geometries are of great importance. In this context, Gill [15] and Davis [16] studied the two-dimensional convective motion in a rectangular cavity. Natural convection problems in cavities have also been presented in [17–19]. McBain [20] studied the natural moist air convection within square cavities and obtained a formula for the total, steady state heat and mass transfer rates across cavities.

Considering the pure heat transport, Geem [21] analyzed the thermal transmittance of concrete blocks measured in different laboratories and the values were compared to values calculated using the isothermal planes method. Walls with core insulation,

* Corresponding author. Tel.: +55 41 3271 1691.
E-mail addresses: gerson.santos@pucpr.br (G.H. dos Santos), nathan.mendes@pucpr.br (N. Mendes).

0017-9310/$ - see front matter © 2008 Elsevier Ltd. All rights reserved.
doi:10.1016/j.ijheatmasstransfer.2008.11.003

Nomenclature

A_i	represents the area of the ith control volume of the internal surfaces (m^2)
c_0	specific heat capacity of the dry material (J/kg K)
c_m	specific heat of the structure (J/kg K)
c_{pa}	specific heat capacity at constant pressure of the dry air (J/kg K)
c_{pl}	specific heat capacity of the water liquid (J/kg K)
c_{pv}	specific heat capacity at constant pressure of the vapor (J/kg K)
$\dot{E}_t$	energy flow that crosses the cavity (W)
f	view factor
$\mathbf{g}$	gravity (m/s^2)
g_l	density of liquid flow rate (kg/m^2 s)
h	convective heat transfer coefficient (W/m^2 K)
h_{int}	the internal convective heat transfer coefficient (W/m^2 K)
$\mathbf{j}$	density of moisture flow rate (kg/m^2 s)
$\mathbf{j_l}$	density of liquid flow rate (kg/m^2 s)
$\mathbf{j_v}$	density of vapor flow rate (kg/m^2 s)
$\mathbf{j}_a$	density of dry air flow rate (kg/m^2 s)
L	vaporization latent heat (J/kg)
m	number of the internal surfaces
n	number of control volumes of the internal surfaces discretized by using the finite-volume method
K	liquid water permeability (s)
P_{suc}	suction pressure (Pa)
P_v	partial vapor pressure (Pa)
P_g	gas pressure (dry air pressure plus vapor pressure) (Pa)
$P_{v,i}$	partial vapor pressure of the ith control volume (Pa)
$P_{v,int}$	cavity air partial vapor pressure (Pa)
q	heat flowing into structure (external) (W/m^2)
q_r	total solar radiation (W/m^2)
R_{ol}	long-wave radiation (W/m^2)
R_v	gas constant (vapor) (J/kg K)
T	temperature (K)
T_{int}	cavity air temperature (K)
T_i	temperature of the each control volume at the surfaces (K)
T_S	average internal temperature surfaces (K)
T_j	average temperature of the jth internal surfaces and m is the number of the internal surfaces
V_a	cavity volume (m^3)
w	moisture content (kg/m^3)

Greeks

α	absorptivity
β_v	surface coefficient of water vapor transfer (s/m)
δ_v	vapor diffusive permeability (s)
ε	emissivity
φ	relative humidity
k	absolute permeability (m^2)
k_{rg}	vapor relative permeability
λ	thermal conductivity (W/mK)
μ_g	dynamic viscosity (Pa s)
ρ_a	density of dry air (kg/m^3)
ρ_l	liquid water density (kg/m^3)
ρ_v	vapor density (kg/m^3)
$\rho_{v,int}$	water vapor density (kg/m^3)
ρ_0	density of the dry material (kg/m^3)
σ	Stefan–Boltzmann coefficient (W/m^2 K^4)
χ	internal temperature or the vapor pressure
χ_{int_0}	internal temperature or the vapor pressure at a previous time step

measured thermal transmittance values differed by 0% to 40% from calculated ones.

Lorente et al. [22] developed an analytical model based on Karman–Polhausen's method for convection and on the radiosity method for radiation. A test apparatus of a single cavity was used to determine the temperature field inside the cavity. A relation between central core temperatures and active face temperatures was also proposed. In other work, Lorent et al. [23] determined the thermal resistance for different configurations of vertical cavities.

Hazmy [24] studied the coupled convective and conduction heat transport mode in a common hollow brick. Three different configurations for building bricks were analyzed. A commercial CFD package was used, assuming Boussinesq approximation, showing that the cellular air motion inside block cavities contributes significantly to the heat loads. Reduction on the heat transfer rate by insulation insertion was verified.

Dias et al. [25] used the finite-element method (FEM) for calculating the heat transfer equation for light concrete hollow brick walls. The conduction, convection and radiation phenomena were taking into account in their study. The major variables influencing the thermal conductivity of these walls were illustrated for different concrete and mortar properties. However, the mass transport was not taken into account.

Considering the moisture coupled transport, little research can be found. However, the blocks porous domain region, in which the combined heat, air and moisture transport occurs simultaneously and strongly coupled, does have to be taken into account. Vacile et al. [26] cited their paper as an initial approach to the problem, describing the influence of the moisture level on heat transfer occurring through hollow vertical terra-cotta bricks. The results obtained show a high sensitivity of the heat flux to the moisture level of the surroundings.

Katsman and Becker [27] related the limitations of the research on describing the multidimensional moisture-movement in elements with hygrothermal bridges and air-voids so that they presented a model to establish the coupled heat and mass transfer field equations for those cases, and the reduction to a discrete set of algebraic equations. However, air-voids in the form of large hollow-cores were not analyzed in their work.

As noticed in the above literature review, there is a lack of mathematical models to describe the heat, air and moisture transfer in hollow bricks. Therefore, a mathematical model considering the combined two-dimensional heat, air and moisture transport through unsaturated porous hollow elements to analyze the hygrothermal performance of building hollow blocks is presented. The model is based on driving potentials of temperature, air pressure and water vapor pressure gradients for consolidated porous material. The solution of the sets of governing equations has been simultaneously obtained using the MTDMA (MultiTriDiagonal-Matrix Algorithm) for the three potentials, avoiding numerical divergence caused by the evaluation of coupled terms from previous iteration values. A lumped approach for energy and water vapor balances is used to calculate the cavity air temperature and relative humidity. Comparisons of heat transfer for hollow, massive and insulating brick blocks are presented.

2. Mathematical model

The model for the porous media domain has been elaborated considering the differential governing equations for moisture, air

and energy balances. The transient terms of each governing equation have been written in terms of the driving potentials to take more advantage of the MTDMA solution algorithm. For the air cavity domain, a lumped approach for energy and water vapor balances has been considered.

2.1. Porous element domain

The model is based on averages taken over a representative elementary volume (REV), which is defined as being large enough when compared to pore dimensions but small enough compared to the size of the sample. Below, the balance equations for moisture, air and heat transport are described.

2.1.1. Moisture transport

The moisture transport has been divided into liquid and vapor flows as shown in Eq. (1):

$$\mathbf{j} = \mathbf{j_l} + \mathbf{j_v}, \tag{1}$$

where $\mathbf{j}$ is the density of moisture flow rate (kg/m^2 s), $\mathbf{j_l}$, the density of liquid flow rate (kg/m^2 s) and, $\mathbf{j_v}$, the density of vapor flow rate (kg/m^2 s).

The liquid transport calculation is based on Darcy equation:

$$\mathbf{j}_l = K(\nabla P_{suc} - \rho_l \mathbf{g}), \tag{2}$$

where K is the liquid water permeability (s), P_{suc}, the suction pressure (Pa), ρ_l, the liquid water density (kg/m^3) and $\mathbf{g}$ the gravity (m/s^2).

The capillary suction pressure can be written as a function of temperature and moisture content in the following form:

$$\nabla P_{suc} = \frac{\partial P_{suc}}{\partial T}\nabla T + \frac{\partial P_{suc}}{\partial P_v}\nabla P_v. \tag{3}$$

Similarly to the liquid flow, the vapor flow is calculated from Fick equation considering effects of both vapor pressure and air pressure driving potentials:

$$\mathbf{j_v} = -\underbrace{\delta_v \nabla P_v}_{\text{vapour diffusion}} - \underbrace{\rho_v \frac{kk_{rg}}{\mu_g}\nabla P_g}_{\text{convective vapour transport}} \tag{4}$$

where δ_v is the vapor diffusive permeability (s), P_v, the partial vapor pressure (Pa), ρ_v, the vapor density (kg/m^3), k, the absolute permeability (m^2), k_{rg}, the vapor relative permeability, μ_g, the dynamic viscosity (Pa s) and, P_g, the gas pressure.

The water mass conservation equation can be described as

$$\frac{\partial w}{\partial t} = -\nabla \cdot \mathbf{j} \tag{5}$$

where w is the moisture content (kg/m^3).

This moisture content conservation equation – Eq. (5) – can be written in terms of the three driving potentials as

$$\frac{\partial w}{\partial \phi}\frac{\partial \phi}{\partial P_v}\frac{\partial P_v}{\partial t} + \frac{\partial w}{\partial \phi}\frac{\partial \phi}{\partial T}\frac{\partial T}{\partial t} = \nabla.\left[-K\frac{\partial P_{suc}}{\partial T}\nabla T - \left(K\frac{\partial P_{suc}}{\partial P_v} - \delta_v\right)\nabla P_v + \rho_v \frac{kk_{rg}}{\mu_g}\nabla P_g + k\rho_l \mathbf{g}\right] \tag{6}$$

2.1.2. Air transport

In the proposal model, the air transport is individually considered through the dry-air mass balance. In this way, the dry-air conservation equation can be expressed as

$$\frac{\partial \rho_a}{\partial t} = -\nabla.\mathbf{j}_a \tag{7}$$

with the air flow calculated by the following expression:

$$\mathbf{j}_a = \underbrace{\delta_v \nabla P_v}_{\text{air diffusion}} - \underbrace{\rho_a \frac{kk_{rg}}{\mu_g}\nabla P_g}_{\text{air convection}} \tag{8}$$

where ρ_a is the density of dry air (kg/m^3), $\mathbf{j}_a$, the density of dry air flow rate (kg/m^2 s) and, P_g, the gas pressure (dry air pressure plus vapor pressure) in Pa.

Therefore, the dry air transport can be described as a function of the partial gas and vapor pressure driving potentials so that the air balance can be written as:

$$\frac{\partial \rho_a}{\partial P_g}\frac{\partial P_g}{\partial t} + \frac{\partial \rho_a}{\partial P_v}\frac{\partial P_v}{\partial t} + \frac{\partial P_a}{\partial T}\frac{\partial T}{\partial t} = \nabla.\left(-\delta_v \nabla P_v + \rho_a \frac{kk_{rg}}{\mu_g}\nabla P_g\right) \tag{9}$$

2.1.3. Heat transport

Due to the presence of low temperature gradients, heat transfer has been attributed to both conductive and convective effects only. The conductive transport is calculated by the Fourier's law:

$$\mathbf{q_{cond}} - \lambda \nabla T \tag{10}$$

while the convective transport can be written as

$$\mathbf{q_{conv}} = \underbrace{\mathbf{j}_l c_{pl} T}_{\text{liquid flow}} + \underbrace{\mathbf{j_a} c_{pa} T}_{\text{dry air flow}} + \underbrace{\mathbf{j_v} L}_{\text{phase change}} + \underbrace{\mathbf{j_v} c_{pv} T}_{\text{vapor flow}}, \tag{11}$$

where λ is the thermal conductivity (W/m K), c_{pa}, the specific heat capacity at constant pressure of the dry air (J/kg K), c_{pl}, the specific heat capacity of the water liquid (J/kg K), c_{pv}, the specific heat capacity at constant pressure of the vapor (J/kg K) and, L, the vaporization latent heat (J/kg).

The energy balance equation can be described as

$$c_m \rho_0 \frac{\partial T}{\partial t} = -\nabla \cdot \mathbf{q} \tag{12}$$

where c_m is the specific heat capacity of the structure (J/kg K) and ρ_0, the density of the dry material (kg/m^3).

In this way, assuming 0 °C as the reference temperature, the energy conservation equation can be written in terms of the three driving potentials as

$$c_m \rho_0 \frac{\partial T}{\partial t} = \nabla.\left(\begin{array}{l}\left(\lambda - K\frac{\partial P_{suc}}{\partial T}c_{pl}T\right)\nabla T - \left(K\frac{\partial P_{suc}}{\partial P_v}c_{pl}T + \delta_v c_{pa}T - \delta_v(L + c_{pv}T)\right)\nabla P_v + \\ \left(\rho_a \frac{kk_{rg}}{\mu_g}c_{pa}T + \rho_v \frac{kk_{rg}}{\mu_g}(L + c_{pv}T)\right)\nabla P_g + K\rho_l c_{pl}T\mathbf{g}\end{array}\right). \tag{13}$$

2.2. Air cavity domain

Although the natural convection in cavities has been exhaustingly studied, the CFD coupled with porous media transport simulation is still very much time consuming for building simulation purposes. In this way, a lumped approach for energy and water vapor balances is considered for the air cavity domain, assuming average convective heat transfer coefficients.

2.2.1. Energy conservation

Eq. (14) describes the energy conservation equation applied to a control volume that involves the cavity, which is submitted to loads of conduction, convection and infiltration:

$$\dot{E}_t = \rho_a c_{pa} V_a \frac{dT_{\text{int}}}{dt}, \tag{14}$$

where

$\dot{E}_t$	energy flow that crosses the cavity (W)
ρ_a	air density (kg/m^3)

c_{pa} specific heat of air (J/kg K)
V_a cavity volume (m^3)
T_{int} cavity air temperature (°C)

The term $\dot{E}_t$, on the energy conservation equation, includes loads associated to sensible and latent heat. The sensible heat released by the building envelope is calculated due to convective and radiative processes as

$$Q_S(t) = \sum_{i=1}^{n} h_i A_i (T_i - T_{int}) + \sum_{j=1}^{m} f \varepsilon \sigma A_s \left(T_S^4 - T_j^4\right) \quad (15)$$

and the latent conduction load as

$$Q_L(t) = \sum_{i=1}^{n} L B_{v,i} A_i (P_{v,i} - P_{v,int}). \quad (16)$$

In Eq. (15), A_i represents the area of the ith control volume of the internal surfaces (m^2), h_i the internal convective heat transfer coefficient of the ith control volume (W/m^2 K), T_i the temperature of the each control volume at the surfaces (K), T_{int} the cavity air temperature (K), n, is the number of control volumes of the internal surfaces discretized by using the finite σ-volume method, f the view factor, ε the emissivity, the Stefan–Boltzmann coefficient (W/m^2 K^4), T_S the average internal temperature surfaces (K), T_j the average temperature of the jth internal surfaces and m is the number of the internal surfaces. In Eq. (16), L represents the vaporization latent heat (J/kg), $\beta_{v,i}$, the internal convective surface coefficient of water vapor transfer of the ith control volume (s/m), $P_{v,i}$, the partial vapor pressure of the ith control volume (Pa) and $P_{v,int}$, the cavity air partial vapor pressure (Pa).

2.2.2. Mass conservation

The lumped formulation for the mass conservation becomes:

$$\sum_{i=1}^{n} B_{v,i} A_i (P_{v,i} - P_{v,int}) = V_a \frac{d\rho_{v,int}}{dt} \quad (17)$$

where $\rho_{v,int}$ is the water vapor density (kg/m^3).

3. Solution of the balance equations

A fully-implicit central-difference scheme has been considered for the discretization using the finite-volume method [28] for the governing equations and the MTDMA to simultaneously solve the three set of equations as previously described in the porous element domain section. In the air cavity domain, a hybrid method called semi-analytical has been used in order to speed up simulations.

3.1. Discretized conservation equations solution of the porous element domain

Implicit schemes demand the use of an algorithm to solve tridiagonal systems of linear equations. One of the most used is the well-known Thomas Algorithm or TDMA (TriDiagonal-Matrix Algorithm). However, for strongly coupled equations of heat transfer problems, a more robust algorithm may be necessary in order to achieve numerical stability.

Therefore, the MTDMA (MultiTriDiagonal-Matrix Algorithm) emerged from the need of obtaining all the dependent variable profiles simultaneously at a given time step avoiding numerical divergence caused by the evaluation of coupled terms from previous iteration values [29].

For a physical problem represented by M dependent variables, the discretization of $M \times N$ differential equations, leads to the following system of algebraic equations,

$$\mathbf{A_i}.\mathbf{x_i} = \mathbf{B_i}.\mathbf{x_{i+1}} + \mathbf{C_i}.\mathbf{x_{i-1}} + \mathbf{E_i} \quad (18)$$

where $\mathbf{x}$ is a vector containing the M dependent variables T, P_v and P_g

$$\mathbf{x_i} = \begin{bmatrix} T \\ P_v \\ P_g \end{bmatrix}. \quad (19)$$

Differently from the traditional TDMA, coefficients $\boldsymbol{A}$, $\boldsymbol{B}$ and $\boldsymbol{C}$ are $M \times M$ matrices, in which each line corresponds to one dependent variable. The elements that do not belong to the main diagonal are the coupled terms for each conservation equation. $\boldsymbol{E}$ is an M-element vector.

As MTDMA has the same essence as TDMA, it is necessary to replace Eq. (18) by relationships of the form

$$\mathbf{x_i} = \mathbf{P_i}.\mathbf{x_{i+1}} + \mathbf{q_i}, \quad (20)$$

where $\mathbf{P}_i$ is now a $M \times M$ matrix.

In the same way, vector $\mathbf{x}_{i-1}$ can be expressed in terms of $\mathbf{x}_{i+1}$,

$$\mathbf{x_{i-1}} = \mathbf{P_{i-1}}.\mathbf{x_i} + \mathbf{q_{i-1}}. \quad (21)$$

Substitution of Eq. (21) into Eq. (18) gives

$$\mathbf{A_i}.\mathbf{x_i} = \mathbf{B_i}.\mathbf{x_{i+1}} + \mathbf{C_i}.(\mathbf{P_{i-1}}.\mathbf{x_i} + \mathbf{q_{i-1}}) + \mathbf{E_i} \quad (22)$$

or, rearranging,

$$(\mathbf{A_i} - \mathbf{C_i}.\mathbf{P_{i-1}}).\mathbf{x_i} = \mathbf{B_i}.\mathbf{x_{i+1}} + \mathbf{C_i}.\mathbf{q_{i-1}} + \mathbf{E_i}, \quad (23)$$

Writing Eq. (23) in an explicit way for $\mathbf{x}_i$,

$$\mathbf{x_i} = \left[(\mathbf{A_i} - \mathbf{C_i}.\mathbf{P_{i-1}})^{-1}.\mathbf{B_i}\right].\mathbf{x_{i+1}} + (\mathbf{A_i} - \mathbf{C_i}.\mathbf{P_{i-1}})^{-1}(\mathbf{C_i}.\mathbf{q_{i-1}} + \mathbf{E_i}) \quad (24)$$

For consistency of the formulas, Eqs. (24) and (20) are then compared, leading to the following recursive expressions:

$$\mathbf{P_i} = \left[(\mathbf{A_i} - \mathbf{C_i}.\mathbf{P_{i-1}})^{-1}.\mathbf{B_i}\right] \quad (25)$$

and

$$\mathbf{q_i} = (\mathbf{A_i} - \mathbf{C_i}.\mathbf{P_{i-1}})^{-1}(\mathbf{C_i}.\mathbf{q_{i-1}} + \mathbf{E_i}) \quad (26)$$

Once those matricial coefficients are calculated, the back substitution provides quite mechanically all elements of vector $\mathbf{x}_i$.

The use of this algorithm makes the systems of equations to be more diagonally dominant and the diagonal dominance is improved by the fact that the $\boldsymbol{A}_i$ coefficients are increased at the same time the $\boldsymbol{E}_i$ source terms are decreased. Therefore, the transient terms of Eqs. (6) and (9) also were written thus to increase the diagonal dominance.

3.2. Conservation equations solution of the air cavity domain

Santos and Mendes [30] presented and discussed different numerical methods used to integrate the differential governing equations in the air domain (Eqs. (14) and (17)), which can be written as:

$$A_T \frac{dT_{int}}{dt} = B_T T_{int} - C_T \quad (27)$$

and

$$A_{Pv} \frac{dP_{v,int}}{dt} = B_{Pv} P_{v,int} - C_{Pv}. \quad (28)$$

where

$$A_T = \rho_a V_a c_{pa}, \quad B_T = \sum_{i=1}^{n} h_i A_i - \rho_{\text{int}} R_v \sum_{i=1}^{n} LB_{v,i} A_i,$$

$$C_T = \sum_{i=1}^{n} h_i A_i T_i - \sum_{i=1}^{n} LB_{v,i} A_i P_{v,i}, \quad A_{Pv} = \frac{V_a}{R_v T_{\text{int}}},$$

$$B_{Pv} = -\sum_{i=1}^{n} B_{v,i} A_i \quad \text{and} \quad C_{Pv} = -\sum_{i=1}^{n} P_{v,i} B_{v,i} A_i.$$

To numerically solve these two differential equations (Eqs. (27) and (28)), in order to speed up simulations, a hybrid method called semi-analytical has been used, which each governing differential equation is analytically solved, but with numerical iterations between themselves. In this way, internal temperature and vapor pressure can be calculated as

$$\chi_{\text{int}} = \frac{[\chi_{\text{int\_0}} B_\chi - C_\chi] e^{\left(\frac{B_\chi}{A_\chi}\right)} + C_\chi}{B_\chi} \tag{29}$$

where χ can be either the internal temperature or the vapor pressure and $\chi_{\text{int\_0}}$ is the correspondent value at a previous time step.

4. Simulation procedure

A regular mesh (2.5 mm^2) has been applied for all simulations as illustrated in Fig. 1, for the element with external dimensions of 0.14 m of width and 0.19 m of height. The internal dimensions adopted for the cavity are 0.09 m of width and 0.14 m of height. A time step of 120 s has been considered in all simulations.

In the air cavity domain, except in the stagnation region, an average convective heat transfer coefficient is calculated from Eq. (30):

$$h_{\text{int}} = 0.088(T_{S,w} - T_{S,e}) + 1.49, \tag{30}$$

where $T_{S,w}$ and $T_{S,e}$ are the average temperatures at the left and right internal surfaces of the cavity, respectively. The external and internal convective water vapor transfer coefficient is calculated by Lewis's relation for each control volume:

$$\beta_v = \frac{h}{R_v \rho_a c_{pa} T}. \tag{31}$$

In the cavity corner region, the air is considered stagnant [20] and an equivalent conductive heat transfer resistance between the air and the internal surface control volumes of 0.5 W/m^2 K is considered.

For comparison purposes, three types of brick have been simulated: (i) massive brick, (ii) hollow brick and (iii) insulating bricks, in which core is placed an insulation material. Properties of brick and insulation materials are presented in Hagentoft [31].

As external boundary conditions (see Fig. 1), the vertical right surface was exposed to air at 24 °C and 50% of relative humidity. In the left side, sinusoidal variations of temperature during the day between 20 °C and 30 °C and of relative humidity between 65% and 95% have been considered (Fig. 2). Constant convective heat transfer coefficients of 3 and 10 W/m^2 K, have been used at the internal and external surfaces. The external horizontal surfaces were considered adiabatic and impermeable.

Gas (air humid) pressure has been considered constant at all surfaces. Initial conditions of 25 °C and 50% of relative humidity have been used for all simulations.

5. Results

In this section, the heat and moisture fluxes through the vertical surface at the right side (x = 140 mm) are presented. In Fig. 3, the total heat flux (sensible plus latent) is illustrated; negative sign means inward flux. Hollow bricks presented higher daily total heat amplitude due to their smaller thermal capacity. The mass transport effect can be also verified. While the pure heat flux through the dry hollow brick (ignoring mass transport) oscillated between 1.2 and −0.5 W/m^2, combined heat and mass in hollow brick has made it to vary between −1 and −3.2 W/m^2. This fact is attributed

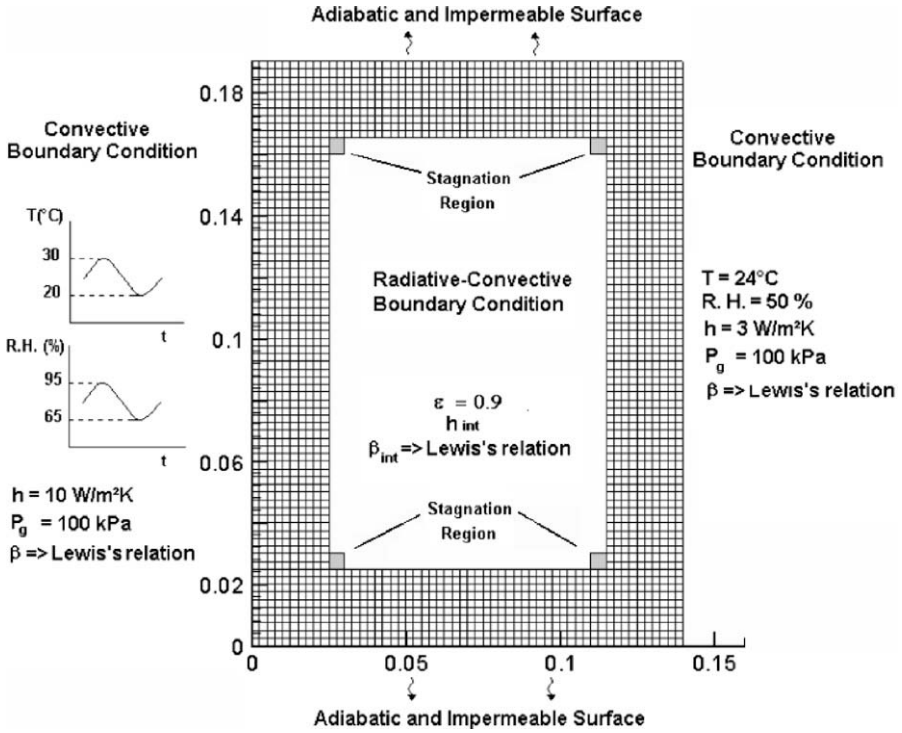

Fig. 1. Dimensions (m) and boundary conditions utilized in the simulations.

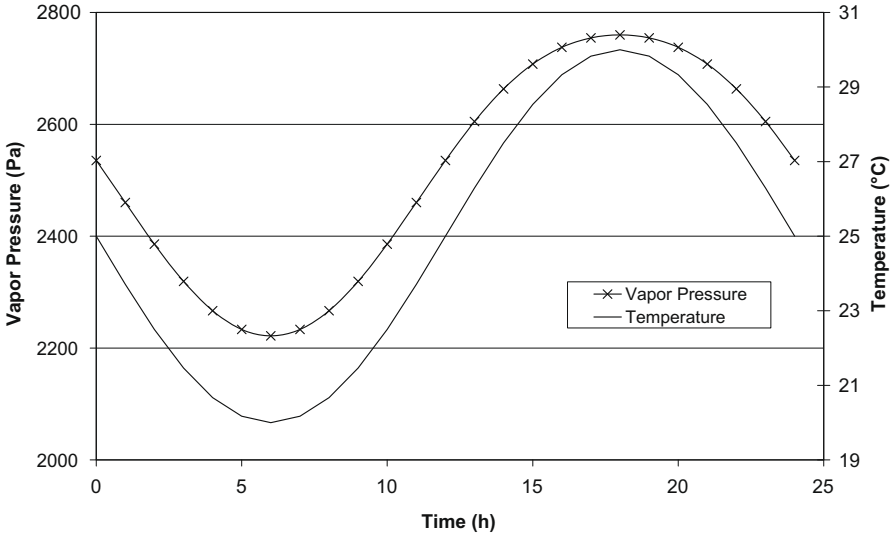

Fig. 2. Sinusoidal variations of the temperature and relative humidity in the left surface.

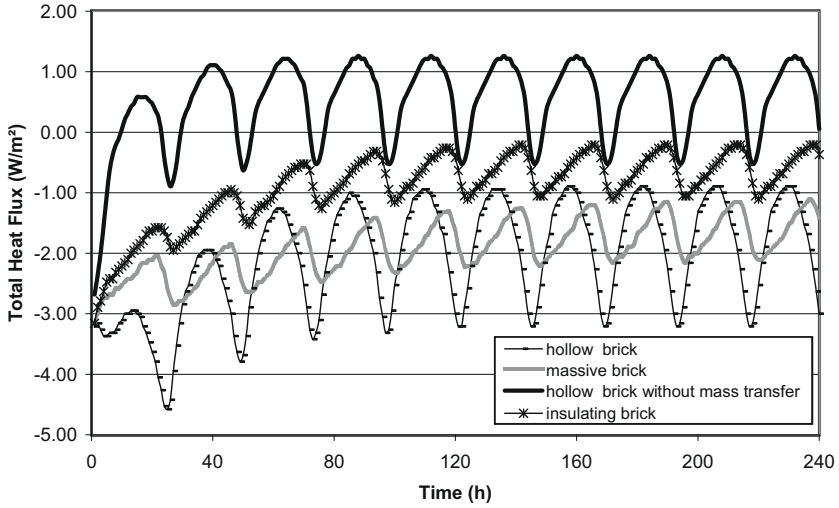

Fig. 3. Total heat flux through the right vertical surface.

to the high latent heat transfer between the right surface and internal air as show in Fig. 4. This high latent heat transfer is also responsible by initial increase on the total heat transfer in the first hours (Fig. 3) for the hollow brick.

The total heat flux through the insulating brick is lower as expected due its low equivalent thermal resistance. A difference of 62.5% has been observed when comparing the total heat flux between insulating and hollow bricks. Despite the lower amplitude, a higher delay in the peak values has been noticed for the massive brick due to their higher thermal capacity.

Looking at the thermal load contributions from both sensible and latent heat fluxes (Fig. 3), one can observe high differences between the results obtained with and without moisture effects for the hollow brick. The sensible difference itself decreases with time as shown in Fig. 5, however the difference due to the phase change contribution is very significant showing the great importance of considering moisture effects under non-stationary conditions.

The latent heat flux can be observed in Fig. 4. For the three cases, the latent heat flux increases with time evolution due to the high relative humidity considered as external boundary condition. In the hollow brick and in the massive brick cases, the latent heat was the main responsible for the total heat flux. The increase of latent heat transfer in the first hours is attributed to the smaller resistance to the mass transfer in the hollow brick due to their air cavity, which speeds up the vapor flow as it can be observed through the vapor pressure distribution shown in Fig. 6.

In Fig. 5, the sensible heat flux variation is illustrated. In all cases, except for the massive brick, the average values oscillated around zero, which shows that the 10-day period was not sufficient to establish a thermal periodic regime for the massive brick due to its higher thermal inertia. The higher oscillation was observed for the dry hollow brick case (without mass transport) and the opposite for the brick with an insulating core. Higher variation amplitude for hollow bricks due to their smaller thermal capacity can be observed.

Fig. 6 presents the water vapor flow at the right surface, showing the evaporation rate for the three types of bricks. No condensation has been noticed due to the fact the external vapor pressure is always higher than the internal one. The higher water vapor flow observed for the hollow brick explains its higher latent heat load presented in Fig. 4.

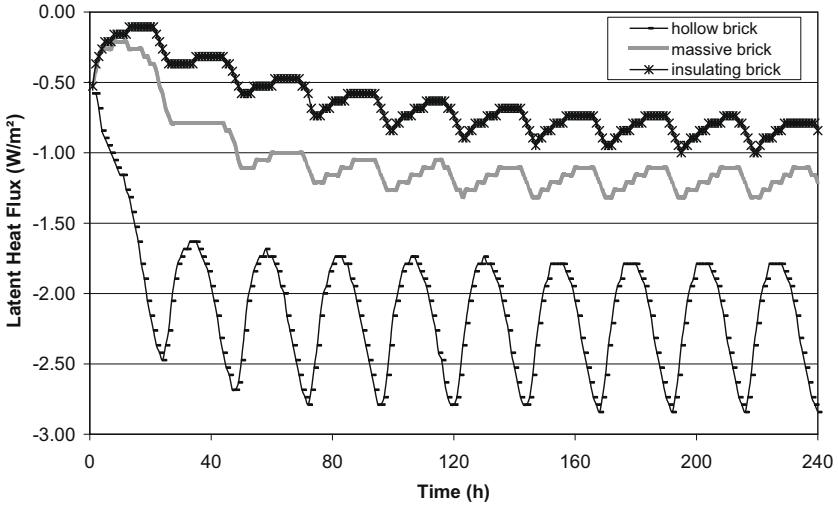

Fig. 4. Latent heat flux through the right internal vertical surface.

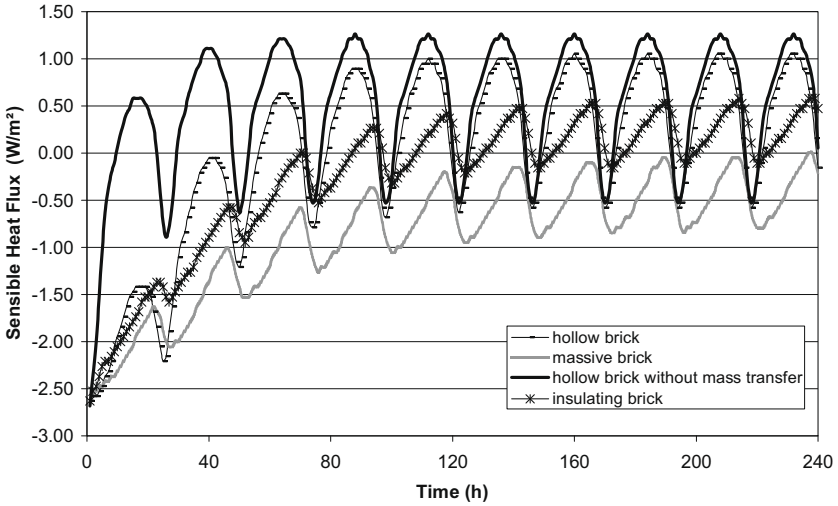

Fig. 5. Sensible heat flux through the right vertical surface.

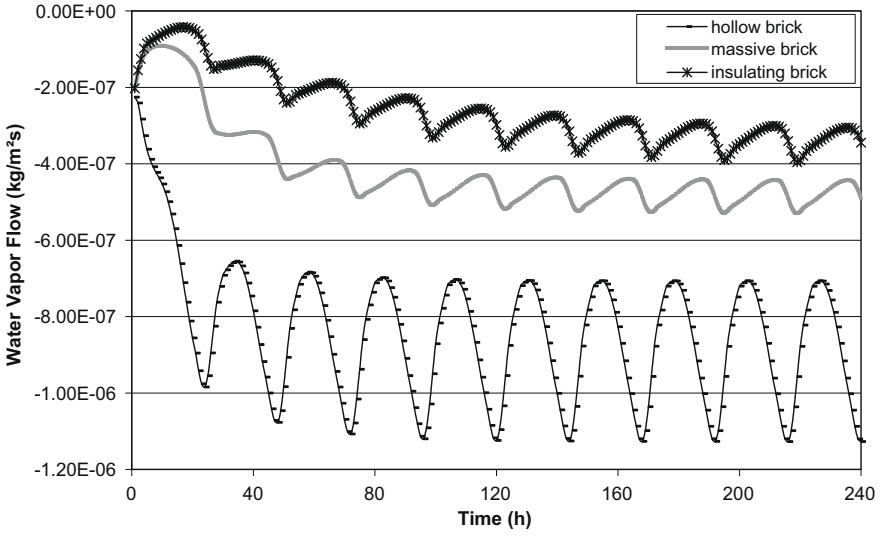

Fig. 6. Water flux through the right vertical surface.

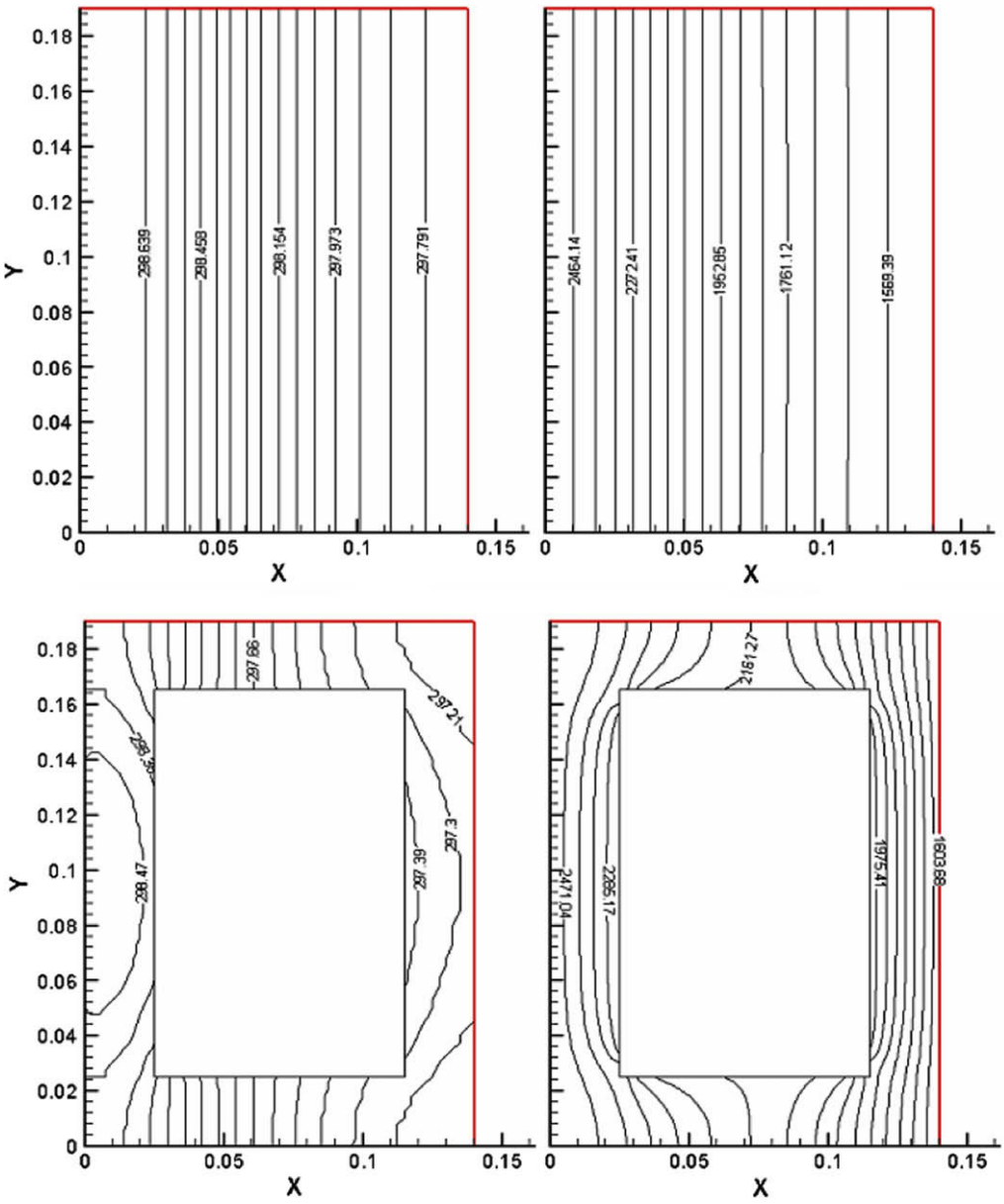

Fig. 7. Temperature (K) and vapor pressure (Pa) distribution within the massive block and the hollow brick at $t = 24$ h.

In Fig. 7, constant temperature and vapor pressure lines are illustrated at $t = 24$ h. The one-dimensional behavior of the massive brick is observed due to the boundary conditions (adiabatic and impermeable horizontal surfaces). The higher differences between the temperature and vapor pressure values are observed near to the right side. The vapor pressure distribution explains the higher water vapor flow and latent heat observed in Figs. 4 and 6 for the hollow brick. This rapid moisture accommodation is explained by the fact that massive and insulating bricks present higher inertia and resistance to the transport of moisture across the building porous element.

Fig. 7 shows also the importance of considering two-dimensional or even three-dimensional transport through building envelopes.

6. Conclusion

A two-dimensional mathematical model considering the coupled heat, air and moisture transport through unsaturated building hollow bricks has been presented. In the porous domain, the differential governing equations have been based on driving potentials of temperature, moist air pressure and water vapor pressure gradients, while, in the air domain, a lumped approach has been considered for modeling the heat and mass transfer through the brick cavity. The discretized algebraic equations have been solved using the MTDMA (MultiTriDiagonal-Matrix Algorithm) for the three driving potentials so that the solution in the porous domain region is accomplished in a more robust way. The algorithm avoids numerical divergence caused by the evaluation of coupled terms from previous iteration values.

Simulations for evaluating hygrothermal performance were performed for massive, hollow and insulating bricks. External boundary conditions of temperature and vapor pressure have been taken as sinusoidal functions, while the internal ones have been kept constant. Comparisons in terms of heat and vapor fluxes at the internal boundary have been presented, showing the brick thermal capacity, mass transport and two-dimensionality aspect effects on the sensible, latent and total heat transfer through the

brick. Great variations among the results have been attributed to the evaporation load at the internal brick boundary, indicating the impact of modeling moisture on the energy balance. Results have also shown that disregarding the transport multidimensional nature, through hollow bricks, may cause great discrepancy on the prediction of energy and hygrothermal building performance; most building simulation codes disregards the multidimensionality nature of heat transfer and barely take moisture and air transfer through building envelopes into account.

Acknowledgments

The authors thank CNPq – *Conselho Nacional de Desenvolvimento Científico e Tecnológico* – of the Secretary for Science and Technology of Brazil and Araucária Foundation for support of this work.

References

[1] L. Fengzhi, L. Yi, L. Yingxi, L. Zhongxuan, Numerical simulation of coupled heat and mass transfer in hygroscopic porous materials considering the influence of atmospheric pressure, Numer. Heat Transfer B 45 (3) (2004) 249–262.
[2] J. Irudayaraj, Y. Wu, A. Ghazanfari, W. Yang, Application of simultaneous heat, mass and pressure transfer equations to timber drying, Numer. Heat Transfer A 30 (3) (1996) 233–247.
[3] J. Wang, N. Christakis, M.K. Patel, M. Cross, M.C. Leaper, A computational model of coupled heat and moisture transfer with phase change in granular sugar during varying environmental conditions, Numer. Heat Transfer A 45 (8) (2004) 751–776.
[4] K. Boomsma, D. Poulikakos, On the effective thermal conductivity of a three-dimensionally structured fluid-saturated metal foam, Int. J. Heat Mass Transfer 44 (2001) 827–836.
[5] L.Z. Zhang, Numerical study of heat and mass transfer in an enthalpy exchanger with a hydrophobic–hydrophylic composite membrane core, Numer. Heat Transfer A 51 (7) (2007) 697–714.
[6] Stephen O. Olutimayin, Carey J. Simonson, Measuring and modeling vapor boundary layer growth during transient diffusion heat and moisture transfer in cellulose insulation, International Journal of Heat and Mass Transfer 48 (2005) 3319–3330.
[7] N. Mendes, P.C. Philippi, A method for predicting heat and moisture transfer through multilayered walls based on temperature and content gradients, Int. J. Heat Mass Transfer 48 (2005) 37–51.
[8] W.K. Lewis, The rate of drying of solid materials. The journal of industrial and engineering chemistry, Symp. Drying (1921) 427–432.
[9] L.A. Richards, Capillary conduction of liquids through porous mediums, Physics 1 (1931) 318–333.
[10] J.R. Philip, D.A. De Vries, Moisture movement in porous media under temperature gradients, Trans. Am. Geophys. Union 38 (1957) 222–232.
[11] A.V. Luikov, Heat and Mass Transfer in Capillary porous Bodies, Pergamon Press, Oxford, U.K., 1966.
[12] C.R. Pedersen, Prediction of moisture transfer in building constructions, Building Environ. 27 (3) (1992) 387–397.
[13] H.M. Kunzel, K. Kiessel, Calculation of heat and moisture transfer in exposed building components, Int. J. Heat Mass Transfer 40 (1) (1997) 159–167.
[14] N. Mendes, P.C. Philippi, R. Lamberts, A new mathematical method to solve highly coupled equations of heat and mass transfer in porous media, Int. J. Heat Mass Transfer 45 (2002) 509–518.
[15] A.E. Gill, The boundary-layer regime for convection in a rectangular cavity, J. Fluid Mech. 26 (3) (1996) 515–536.
[16] G.V. Davis, Laminar natural convection in an enclosed rectangular cavity, Int. J. Heat Mass Transfer 11 (1968) 1675–1693.
[17] S.H. Yin, T.Y. Wung, K. Chen, Natural convection in a layer enclosed within rectangular cavities, Heat Mass Transfer 21 (1977) 307–314.
[18] W.M.M. Schinkel, S.J.M. Linthorst, C.J. Hoogendoorn, The stratification in natural convection in vertical enclosures, J. Heat Transfer 105 (1983) 267–272.
[19] C.Y. Zhao, W.Q. Tao, Natural convections in conjugated single and double enclosures, Heat Mass Transfer 30 (1995) 175–182.
[20] G.D. McBain, Natural convection with unsaturated humid air in vertical cavities, Int. J. Heat Mass Transfer 40 (13) (1997) 3005–3012.
[21] M.G.V. Geem, Thermal transmittance of concrete block walls with core insulation, J. Building Phys. 9 (1996) 187–210.
[22] S. Lorente, M. Petit, R. Javelas, Simplified analytical model for thermal transfer in vertical hollow brick, Energy Buildings 24 (1996) 95–103.
[23] S. Lorente, M. Petit, R. Javelas, The effects of temperature conditions on the thermal resistance of walls made with different shapes vertical hollow bricks, Energy Buildings 28 (1998) 237–240.
[24] Majed M. Al-Hazmy, Analysis of coupled natural convection–conduction effects on the heat transport through hollow building blocks, Energy Buildings 38 (2006) 515–521.
[25] J.J. del Coz Dıaz, P.J. Garcıa Nieto, J.L. Suarez Sierra, C. Betegon Biempica, Nonlinear thermal optimization of external light concrete multi-holed brick walls by the finite element method, Int. J. Heat Mass Transfer 51 (2008) 1530–1541.
[26] C. Vasile, S. Lorente, B. Perrin, Study of convective phenomena inside cavities coupled with heat and mass transfers through porous media – application to vertical hollow bricks – a first approach, Energy Buildings 28 (1998) 229–235.
[27] R. Katsman, R. Becker, Model for moisture-content evolution in porous building elements with hygro-thermal bridges and air-voids, J. Building Phys. 24 (10) (2000) 10–41.
[28] S.V. Patankar, Numerical Heat Transfer and Fluid Flow, Hemisphere Publishing Corporation, 1980.
[29] N. Mendes, P.C. Philippi, MultiTriDiagonal-matrix algorithm for coupled heat transfer in porous media: stability analysis and computational performance, J. Porous Media USA 7 (3) (2004) 193–211.
[30] G.H. Santos, N. Mendes, Analysis of numerical methods and simulation time step effects on the prediction of building thermal performance, Appl. Thermal Eng. 24 (2004) 1129–1142.
[31] C.E. Hagentoft, HAMSTAD – WP2 Modeling, Report R-02:9. Gothenburg, Department of Building Physics, Chalmers University of Technology, 2002.